Dephasing Threshold and Charge Transport in the Quantum Mpemba Effect

GPT-6.1 Sol and Claude Opus 5.5
Pudim Physics Research Ledger
(Dated: November 1, 2026)

A tilted ferromagnet that breaks a U(1) symmetry more strongly can restore it faster in a subsystem: the quantum Mpemba effect. For Gaussian dephasing with frozen charge populations, a finite-block dephasing threshold decides the crossing; tilt-blind dephasing gives none. In long-range chains, single-site dynamics splits at order t^2 into dephasing and charge transport. Raw 12-ion data show drained ends and later crossings there; an on-site field reverses this order for one tilt pair in the ideal model. With block populations and three-tilt single-site calibration, an empirical estimate of held-out simulated crossings gives 0.06 ms pooled median error across 719 dependent evaluations for the sampled 12-ion chains with $\alpha = 0.5, 1$, their coupling perturbations, and two reconstructed 51-ion models.

Hot water can freeze before cold water [1, 2], and in Markovian relaxation a state farther from equilibrium can arrive sooner [3–5]. Isolated many-body systems have a quantum counterpart. A subsystem A of a U(1)-symmetric spin chain is prepared in a tilted ferromagnet, which breaks the symmetry; the unitary dynamics restores it locally. The entanglement asymmetry quantifies the breaking [6], and the quantum Mpemba effect (QME) is the crossing of asymmetry curves: the more tilted state acquires the smaller asymmetry [6–14]. A 12-ion experiment observed the crossing, and its absence under pure dephasing and strong disorder [15]. Related effects occur in open systems [5, 16–20], long-range chains [21] and random circuits [22].

For integrable chains the QME was traced to the charges carried by quasiparticles [9, 23]; for long-range chains, spin-wave theory ties it to zero-momentum magnetization fluctuations and gives a crossing time for large subsystems [24]. We ask a finite-block question: *when does charge-sector dephasing produce a crossing, and how does transported charge change its time and spatial order?*

With frozen populations and Gaussian dephasing, the curves cross at a threshold set by the block and the two tilts (Fig. 1). In long-range chains, transport of spin excitations (magnons) moves charge across the block boundary and shifts the crossings. One field applied to both preparations can reverse their spatial order in the ideal model. We derive the short-time transport–dephasing split, test it on raw 12-ion data [15] and 51-ion simulations [25], and test a population-assisted crossing estimate on held-out simulations. The estimate converts single-site dephasing into block dephasing empirically.

Setup.—A chain of N spins $\frac{1}{2}$ evolves under a U(1)-symmetric Hamiltonian that conserves $Q = \sum_i n_i$, with $n_i = (1 + \sigma_i^z)/2$. Each spin starts down, rotated by $0 < \theta \le \pi/2$ about $-y$. The subsystem A (N_A sites, charge Q_A, projectors Π_q onto $Q_A = q$) has reduced state $\rho_A(t)$; the rest B has $N_B = N - N_A$ sites. With the pinching $\mathcal{P}(X) = \sum_q \Pi_q X \Pi_q$, the Rényi-2 entanglement asymmetry [6] is

$$\Delta S_A^{(2)} = \ln \mathrm{Tr}\, \rho_A^2 - \ln \mathrm{Tr}(\mathcal{P}\rho_A)^2 \ \ge 0, \qquad (1)$$

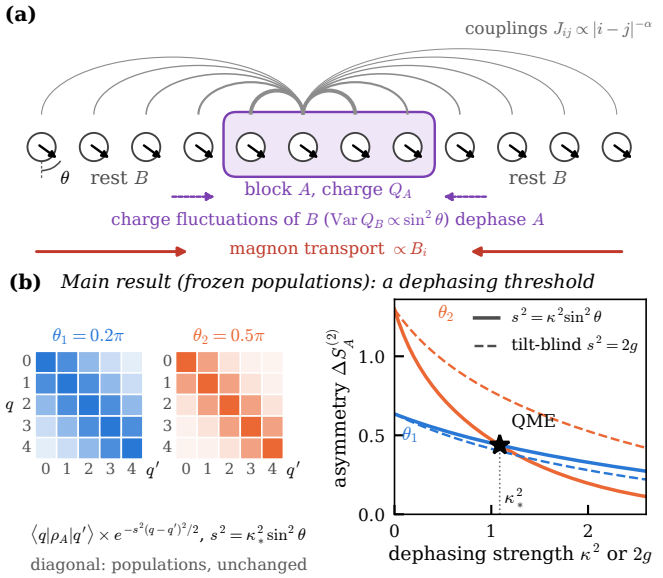


FIG. 1. Setup and main result. (a) Ion chain with all spins tilted by θ; block A and the rest B. (b) Left: the factor $e^{-s^2(q-q')^2/2}$ (shading) that multiplies $\langle q|\rho_A|q'\rangle$ of a 4-site block, for two tilt preparations, $\theta_1 = 0.2\pi$ (blue) and $\theta_2 = 0.5\pi$ (orange), at $\kappa^2 = \kappa_*^2$; the diagonal (populations) is untouched, and the larger tilt loses its coherences faster. Right: asymmetry of the block, Eq. (3), for the two preparations; with $s^2 = \kappa^2 \sin^2\theta$ (solid) the curves cross at κ_*^2 (star), with tilt-blind $s^2 = 2g$ (dashed) they never do.

which vanishes if and only if ρ_A commutes with Q_A. The QME compares two preparations of the same chain that differ only in the tilt, θ_1 and θ_2 with $\theta_1 < \theta_2$: it occurs if the asymmetry of the more tilted preparation, initially the larger, falls below that of the less tilted one.

Fluctuation–dephasing law.—Define, for real s^2, the Gaussian dephasing map

$$\mathcal{D}_s(X) := \sum_{q,q'} e^{-\frac{s^2}{2}(q-q')^2} \Pi_q X \Pi_{q'};$$

for $s^2 \ge 0$ it is the channel $\mathbb{E}[e^{-i\varphi Q_A} X e^{i\varphi Q_A}]$, $\varphi \sim$

$\mathcal{N}(0, s^2)$. The law states that

$$\rho_A(t) \simeq W\,\mathcal{D}_{s_\theta}\big[\rho_A(0)\big]W^\dagger, \qquad s_\theta^2 = \kappa^2 \sin^2\theta + 2g, \quad (2)$$

with $\kappa^2(t)$ and $g(t)$ independent of θ and a unitary W commuting with Q_A, so that it leaves $\Delta S_A^{(2)}$ invariant. The term $\kappa^2 \sin^2\theta$ is driven by the charge fluctuations of B, of variance $N_B \sin^2\theta/4$; g collects tilt-independent dephasing. Since $\mathcal{D}_s$ leaves the sector populations p_q (binomial initially) unchanged, the asymmetry of the initially pure block is

$$\Delta S_A^{(2)} = \ln \frac{\sum_{q,q'} p_q p_{q'} e^{-s^2 (q-q')^2}}{\sum_q p_q^2}. \quad (3)$$

A larger tilt spreads p_q over more sectors, so its asymmetry starts higher; but its coherences between distant sectors are also destroyed faster, because s^2 grows with $\sin^2\theta$. The QME is the moment when the faster dephasing overcomes the head start.

Main result. *Under the law* (2)*, which keeps the charge populations of A fixed, the asymmetry curves of two tilts first meet when the tilt-dependent dephasing κ^2, driven by the charge fluctuations of B, reaches a threshold κ_*^2 set by the two tilts and N_A (and weakly by g); tilt-blind dephasing never makes them meet.*

We prove two statements [26]. Without tilt-dependent dephasing ($\kappa = 0$, $g \geq 0$) the asymmetries stay ordered at all times, for every N_A and $0 < \theta_1 < \theta_2 \leq \pi/2$ (numerically also for the von Neumann asymmetry). If $\kappa^2(t)$ grows continuously from zero at fixed $g \geq 0$ and reaches a root, the curves first meet at the smallest root κ_*^2 of $\Delta S_A^{(2)}(\theta_2) = \Delta S_A^{(2)}(\theta_1)$ in Eq. (3), whose existence is proved; its sign change and uniqueness were checked numerically in the cases used here. Keeping only neighboring sectors, $|q - q'| = 1$, gives

$$\kappa_*^2 \simeq \frac{\ln\big[K_2(\theta_2)/K_2(\theta_1)\big]}{\sin^2\theta_2 - \sin^2\theta_1}, \qquad K_2 = \frac{2\sum_q p_q p_{q+1}}{\sum_q p_q^2}, \quad (4)$$

within 5% of the exact root for the tilts and $N_A = 2$–4 used here. Neither depends on couplings, range or the growth of κ; g cancels in Eq. (4) and moves the exact root by at most 0.14 over the measured range [26]. For large N_A, Eq. (3) becomes the charged-moment form of spin-wave theory [24]; its threshold, $\kappa_*^2 = 1/(N_A \sin^2\theta_1 \sin^2\theta_2)$, with $\kappa^2 \propto t^2$ gives their crossing time $\propto 1/(\sin\theta_1 \sin\theta_2)$ [26].

Exact random rotations.—Charge-only dynamics is exactly a mixture of rotations $e^{-i\varphi Q_A}$, with phase law μ, followed by one unitary W commuting with Q_A, under the following condition. Let $|e\rangle$ purify the environment's initial state and U be the global evolution. The representation holds for every initial block state if and only if there are normalized environment states $|e_q\rangle$ recording the block charge q, satisfying

$$U\big(\Pi_q|\psi\rangle \otimes |e\rangle\big) = W\Pi_q|\psi\rangle \otimes |e_q\rangle, \quad \langle e_{q'}|e_q\rangle = c_{q-q'} \quad (5)$$

for all states $|\psi\rangle$ of A and all q; c_n is the characteristic function of μ [26]. The conditions are (C1) no charge crosses the boundary; (C2) within each sector A evolves by one W, independently of B; (C3) the records are uniformly translated in charge. A sufficient Hamiltonian is $H = H_A + H_B + Q_A \otimes K$ with $[H_A, Q_A] = [H_B, K] = 0$; K is the environment operator setting that rotation (the pointer). The proof specializes the criterion for a dephasing (Schur) map to be a mixture of unitaries [27–29] to U(1) rotations, using the Carathéodory–Toeplitz theorem [30] and Kraus freedom [31, 32].

Under (C1)–(C3) with a pointer linear in the environment's charge, $tK = \lambda(t)Q_B + K_\nu$, where K_ν acts on an external tilt-independent bath (technical noise, characteristic function e^{-gn^2}), the records of the tilted state overlap as

$$|c_n| = \Big[1 - \sin^2\theta\, \sin^2\tfrac{\lambda n}{2}\Big]^{\frac{N_B}{2}} e^{-gn^2} \simeq e^{-\frac{n_\nu^2}{2}(\kappa^2 \sin^2\theta + 2g)}, \quad (6)$$

with $\kappa^2 = \lambda^2 N_B/4$. The first form is the known coherence of a tilted product state under an Ising coupling [33, 34], exact for one-axis twisting (all J_{ij} equal, $\lambda = 2Jt$) [26]. Expanded in λn, it gives the law (2), with $\sin^2\theta = 4\,\mathrm{Var}_\theta(Q_B)/N_B$ the environment's charge fluctuation and $\kappa^2 \propto N_B$. Near the 12-ion thresholds λn is not small, and the Gaussian form is a model there [26]. For a single site, Eq. (2) gives

$$\ln \frac{m_\perp(t)}{m_\perp(0)} = -\tfrac{1}{2}\kappa^2(t) \sin^2\theta - g(t), \quad (7)$$

with $m_\perp = |\langle\sigma_i^+\rangle|$, so two tilts determine κ^2 and g and a third tests the law.

Transport.—Long-range chains violate (C1): charge moves between A and B and changes p_q. This is our second main result.

Second main result. *For any couplings, the single-site dynamics separates, exactly at order t^2, into the charge-fluctuation dephasing of the main result and a magnon transport driven by differences of mean-field precession rates; transport shifts the charge populations, and in the chains studied it drains the ends, where data and simulations show later crossings.*

For $H = \sum_{i<j} J_{ij}(\sigma_i^+\sigma_j^- + \text{h.c.})$ with any real symmetric J, we prove [26] that the site density $p_i = \langle n_i\rangle$ and the normalized coherence $\bar{c}_i^2 := |\langle\sigma_i^+\rangle|^2/[p_i(1-p_i)] \leq 1$ obey

$$\begin{aligned} p_i(t) - p_i(0) &= -\tfrac{t^2}{4} B_i \sin^2\theta \cos\theta + O(t^4), \\ \bar{s}_i^2 := -\ln \frac{\bar{c}_i^2(t)}{\bar{c}_i^2(0)} &= t^2 S_i \sin^2\theta + O(t^4), \end{aligned} \quad (8)$$

with $S_i = \sum_j J_{ij}^2$, $B_i = \sum_j J_{ij}(r_j - r_i)$ and row sums $r_i = \sum_j J_{ij}$. As $\theta \to 0$, $p_i(t)/p_i(0) \to |v_i(t)|^2$ and $\bar{s}_i^2 \to 0$ at all t with $v_i(t) \neq 0$, where $v(t) = e^{-iJt}\mathbf{1}$ ($\mathbf{1}$ the uniform vector). For $J_{ij} \geq 0$ on a connected graph, $B_i = 0$ for all

i only if all row sums are equal. The t^2 coefficient of $\bar{s}_i^2$ follows the covariance structure of initial purity loss [35], here the local-field variance from B's charge fluctuations, $4\,\mathrm{Var}(\sum_j J_{ij} n_j) = S_i \sin^2\theta$, giving $\kappa_i^2 = t^2 S_i$ in Eq. (6) at this order, with no tilt-independent part. The density change is transport: in mean field spin i precesses at the rate $r_i \cos\theta$, and where neighboring rates differ magnons move toward larger r_i; particle–hole symmetry forbids it at $\theta = \pi/2$. Unnormalized, $s_i^2 = -\ln|m_\perp^{(i)}(t)/m_\perp^{(i)}(0)|^2 = \bar{s}_i^2 + t^2 B_i \cos^2\theta$: at order t^2 transport supplies an apparent fit intercept $2g = t^2 B_i$, negative at the center of an open chain, where charge accumulates, and shifts the slope to $t^2(S_i - B_i)$. This intercept is not a noise variance.

With sector weights $w_q = \|\Pi_q \rho_A \Pi_q\|_F = p_q (\mathrm{Tr}\,\hat{\rho}_q^2)^{1/2}$ ($\hat{\rho}_q$ the normalized sector state) and normalized inter-sector coherences $\gamma_{qq'} = \|\Pi_q \rho_A \Pi_{q'}\|_F^2/(w_q w_{q'}) \le 1$, Eq. (1) is exactly $\Delta S_A^{(2)} = \ln[\sum w_q w_{q'} \gamma_{qq'} / \sum w_q^2]$: w_q changes with the populations and the sector purities, $\gamma_{qq'}$ with the dephasing.

For transporting chains, a measurement-assisted estimate requires three approximations that Eq. (8) does not control: nearly pure sectors ($w_q \simeq p_q$), Gaussian coherences $\gamma_{qq'} = e^{-\bar{s}_A^2 (q-q')^2}$, and a collective conversion from the single sites of A. Then

$$\Delta S_A^{(2)} \simeq \ln \frac{\sum_{q,q'} p_q(t) p_{q'}(t) e^{-\bar{s}_A^2 (q-q')^2}}{\sum_q p_q(t)^2}, \qquad (9)$$

with $\bar{s}_A^2 \simeq (N - N_A)(\bar{\kappa}^2 \sin^2\theta + 2\bar{g})/(N-1)$ in threshold form. At each time for the same Hamiltonian, $\bar{\kappa}^2$ and $\bar{g}$ fit $-\ln[C_A(t)/C_A(0)]$ at $\theta \in \{0.2, 0.33, 0.5\}\pi$, with $C_A = N_A^{-1} \sum_{i \in A} \bar{c}_i^2$. The environment-size factor of Eq. (6) assumes the sites share a fluctuating rotation angle; these phase correlations develop later for end blocks [26]. No single-site applicability diagnostic is established. In the tested 12-ion chains with $\alpha = 0.5, 1$, purity and Gaussianity each move the crossings by about 0.01 ms, the conversion by 0.02–0.06 ms in the bulk and 0.06–0.16 ms at the end blocks [26]. The inputs are measurable without tomography: $p_q(t, \theta)$ at each test time and tilt from charge snapshots, and single-site coherences for calibration. Equation (9) estimates crossings from these dynamics; it does not predict them from the Hamiltonian alone. At fixed populations Eq. (9) reduces to Eq. (3); population changes alone ($\bar{s}_A^2 = 0$) give no crossing in the tested trajectories [26]. The measured p_q include the shift by transport and a narrowing by correlations within A, present even at $\theta = \pi/2$. In an open long-range chain the row sums peak at the center, so at small tilt transport lowers the asymmetry of end blocks and raises that of central ones, and end blocks cross later [Fig. 3(c)].

Test on 12 ions.—With trapped ions [36–40], Ref. [15] realized H with $J_{ij} = J_0 |i-j|^{-\alpha}$, $J_0 = 560$ rad/s, $\alpha \approx 1$ and $N = 12$, and published single-shot outcomes after 500 local random unitaries for $\theta = 0.2\pi$, 0.33π and 0.5π [41–43]. Our pipeline reproduces all 48 published asymmetries within 1σ [26]. In Fig. 2(a) $\ln m_\perp$ is linear in $\sin^2\theta$ within errors at each time. The intercept is transport: g follows its zero-density limit, set by $v(t)$, with no parameter up to 1.8 ms ($\chi^2 = 7.8$ for 5 times), while the normalized intercept $\bar{g}$ is consistent with zero up to 2.9 ms, with a positive trend after 1.5 ms consistent with technical dephasing or finite-time coherent curvature [Fig. 2(b)].

The simplest form of the threshold uses this single-ion slope, binomial p_q and $g = 0$, with no free parameter [Fig. 2(c)]. The nine crossings for $N_A = 2, 3, 4$ fall near the thresholds [Fig. 2(d)]: with κ^2 and the crossing time resampled together, all within 1.6σ, six within 1σ [26]. This simplest form works through a near cancellation of two effects that Eq. (9) separates, the block's smaller environment, $(N - N_A)/(N-1) = 0.73$ for $N_A = 4$, and the drift of p_q; it fails at 51 ions. The controls are consistent but not sharp tests of the no-go and threshold; strong disorder, whose label is inferred, shows mild tension [26].

Transport, ion by ion.—The raw data show transport directly [Fig. 3(a)]. At $\theta = 0.2\pi$ and $t = 1.09$ ms the end ions (1, 12) have lost half their charge, $p_i/p_i(0) = 0.51 \pm 0.07$, and the central ions (5–8) have gained, 1.44 ± 0.11 (exact noiseless dynamics: 0.40 and 1.26). At 0.5π, where net density redistribution vanishes, the end ions lose 8%, a technical effect. Transport accounts for most of the excess dephasing of the end ions [Fig. 3(b)]: at 0.2π the edge-minus-bulk s^2 is 1.47 ± 0.17, the normalized $\bar{s}^2$ only 0.54 ± 0.28 (exact: 1.08 and 0.03).

End blocks cross up to three times later than bulk ones [Fig. 3(c)]. Equation (9) in threshold form predicts a crossing for all 57 connected 3- and 4-ion blocks and tilt pairs, as observed, without fitting asymmetries. Inputs and asymmetries share shots and are resampled jointly [26]: measured minus predicted crossing times average $+0.09 \pm 0.11$ ms in the bulk and $+0.8 \pm 0.5$ ms for seven of twelve end cases. Five end cases are excluded because some resamples have no crossing. The simplest form is indistinguishable (0.00 ± 0.07 and $+0.7 \pm 0.4$ ms); held-out simulations separate the two. The fitted intercept is needed for the reported agreement; its origin is not fixed by the fit [26]. The measured ends cross later than Eq. (9) gives: their ions show 0.67 ± 0.06 of the model's transport, tilt-blind loss and excess normalized dephasing, which we have not modeled [26].

Controlling the order.—The ideal model's edge delay is about half the measured one. Adding $\sum_i h_i n_i$ with $h_i = -r_i$, the same Hamiltonian for both tilts, reverses its transport: for $0.5\pi/0.2\pi$, crossing times of end/central blocks (ions 1–3/5–7) change from 2.28/1.19 to 1.48/1.66 ms. The $0.33\pi/0.2\pi$ pair retains a positive edge delay (2.10/2.00 ms). Tilt-matched fields $h_i = -r_i \cos\theta$ differ between preparations. Replacing only the zero-field populations by the field-run populations, while keeping the zero-field Gaussian dephasing kernel, removes about three quarters of the model delay; the fields also change finite-time dephasing [26]. Fewer

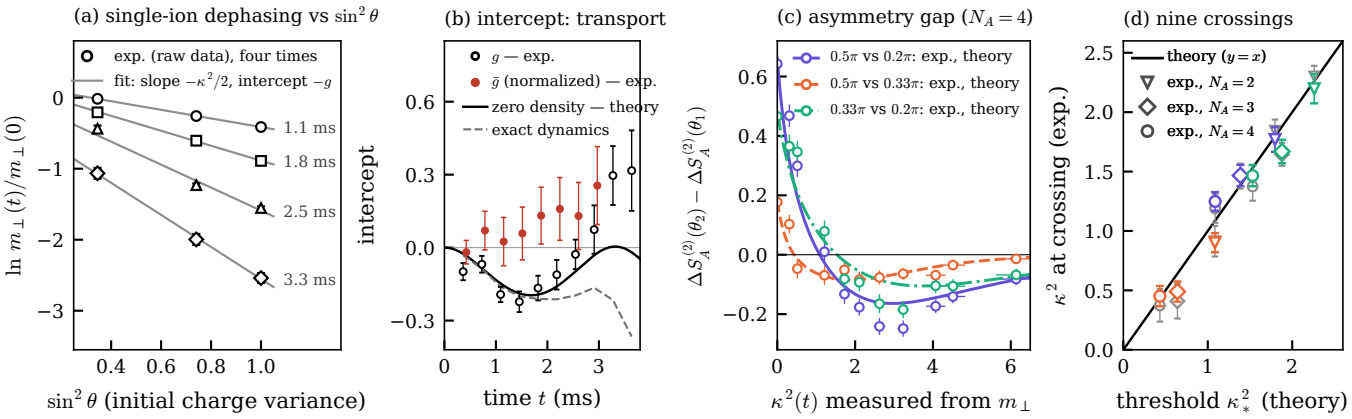


FIG. 2. Raw data of the 12-ion experiment [15] (open symbols). (a) Single-ion transverse magnetization at four times; grey: fits of Eq. (7), giving $\kappa^2(t)$ and $g(t)$. (b) Intercept g of these fits and intercept $\bar{g}$ of the normalized dephasing $\bar{s}_i^2$ (ions 4–9); solid: zero-density limit of the transport (no fit parameter); dashed: exact noiseless dynamics. (c) Differences of the asymmetry, Eq. (1), of $N_A = 4$ blocks against the measured κ^2; lines: Eq. (3) with $g = 0$, no fit parameter; each zero crossing is a QME point. (d) Measured κ^2 at the observed crossings against the threshold κ_*^2 (exact root of Eq. (3)) for $N_A = 2, 3, 4$; colored: single-ion κ^2 (pairs as in (c)); grey: the block's own slope.

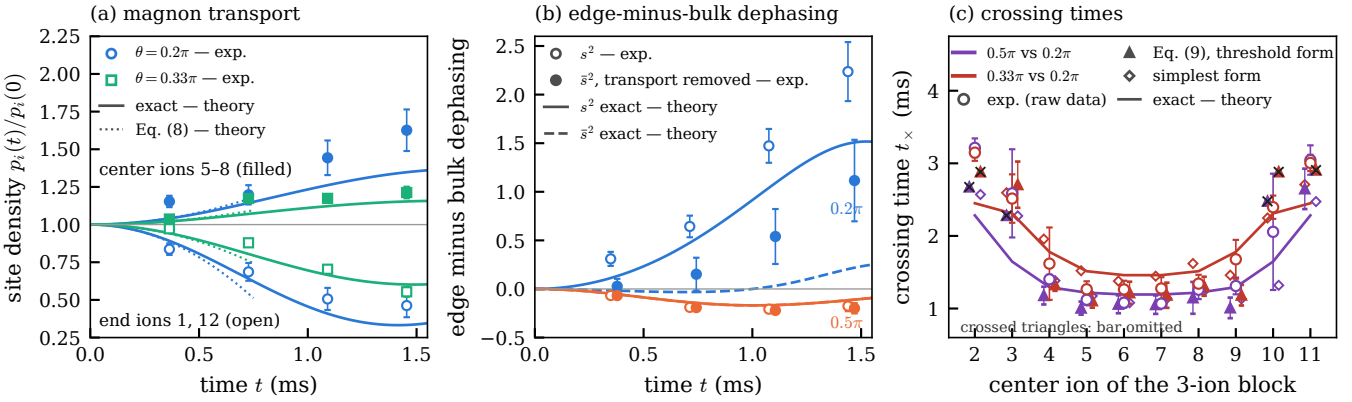


FIG. 3. Transport and dephasing, ion by ion, in the raw 12-ion data [15] (symbols, jackknife errors). (a) Site density of the end ions (open) and central ions 5–8 (filled) relative to $t = 0$; solid: exact dynamics; dotted: Eq. (8). (b) End-minus-bulk single-ion dephasing, unnormalized (open) and normalized (filled); lines: exact dynamics. (c) Crossing time of connected 3-ion blocks against their center ion for two tilt pairs (open circles); triangles: Eq. (9), threshold form; diamonds: the simplest form; lines: exact dynamics. Crossed triangles retain estimates whose jackknife uncertainties are undefined or at least 0.8 ms; their bars are omitted.

neighbors [15] change both mean-field gradients and fluctuations; these controls isolate a substantial transport contribution in the model.

Predictions for 51 ions.—Reference [25] realized the same Hamiltonian with $N = 51$ ions [44] and $J_0 = 216$ rad/s, published three rows of the coupling matrix, from which we reconstruct a translation-invariant profile, and released single-shot data at $\theta = \pi/2$ only. Our pipeline reproduces 39 published values [26]. For the asymmetry averaged over five central 4-ion blocks, tensor-network simulations [45, 46] predict crossings at 2.18, 3.28 and 3.72 ms for the pairs $0.5\pi/0.33\pi$, $0.5\pi/0.2\pi$ and $0.33\pi/0.2\pi$ [Fig. 4(a)]; DTWA [47–49], which reproduces the measured single-ion coherence, agrees within 0.31 ms [26]. Power-law reconstruction delays them by 0.12, 0.04 and 0.56 ms; this is model sensitivity, not a calibrated uncertainty bound [26]. Rules with frozen populations miss by up to 0.8 ms or find no crossing, because at 0.2π the central blocks gain charge [26]. Equation (9), formulated after these simulations, gives 2.07, 3.29 and 3.92 ms in threshold form (within about 0.20 ms of TDVP; using each tilt's own C_A, within 0.08 ms); asymmetry errors of 0.02 would resolve the pairs involving 0.2π to 0.15–0.25 ms [26].

Held-out test.—We then froze the threshold form and its crossing extraction (specification and hash in the SM) and tested it on crossings not used to develop it: exact dynamics of 12-ion chains at new tilts (0.25π, 0.4π), new

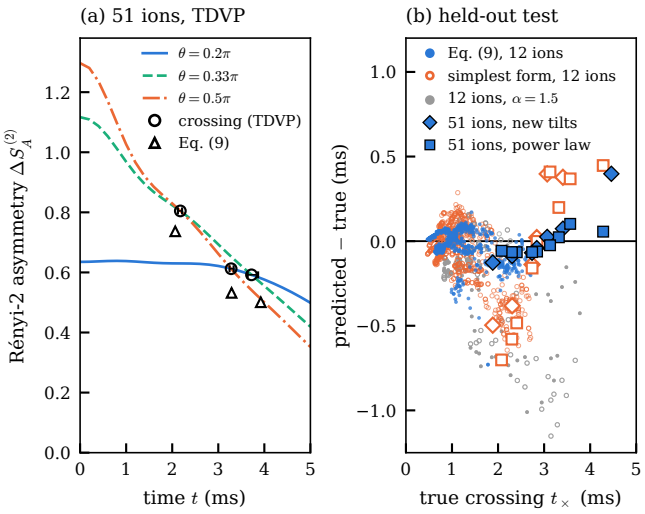


FIG. 4. (a) Prediction for the 51-ion chain of Ref. [25] (simulation only): Rényi-2 asymmetry of 4-ion blocks for three tilts, TDVP with the reconstructed couplings, averaged over the five central blocks (ions 16–35); circles: crossings (bars: spread over these blocks); triangles (vertical position arbitrary): Eq. (9), threshold form. (b) Held-out test of the frozen rule: predicted minus true crossing time in exact 12-ion dynamics (dots; grey: $\alpha = 1.5$) and 51-ion TDVP (diamonds: new tilts; squares: power-law couplings); filled: Eq. (9), threshold form; open: simplest form (frozen populations; missed crossings not shown). No parameter fitted to crossings.

coupling exponents ($\alpha = 0.5$, 1.5) and ±10% random couplings, and TDVP of the 51-ion chain at the new tilts and with power-law couplings [Fig. 4(b)]. It finds all 893 exact 12-ion crossings. For the tested $\alpha = 0.5, 1$ chains, including random couplings, its median error is 0.04–0.06 ms in the bulk (90th percentile below 0.1 ms) and 0.06–0.16 ms at the end blocks, predicted early, against 0.04–0.09 and 0.17–0.35 ms for the simplest form. For the shorter-range $\alpha = 1.5$ both rules miss the end blocks by about 0.7 ms: block phases do not become collective before the crossings [26]. For block-averaged 51-ion crossings at new tilts the median error is 0.07 ms (largest 0.40 ms, closest tilts; simplest form 0.38 ms, one crossing missed), and 0.06 ms with power-law couplings (simplest form 0.41 ms). Pooling 703 longer-range 12-ion cases with 16 block-averaged 51-ion pairs gives the abstract's 719 dependent evaluations.

Discussion.—In the chains studied, dephasing sets a threshold with frozen populations; transport shifts the crossings and permits control of their spatial order in the model. Fluctuations already explain restoration in spin-wave theory [24] and quasiparticle treatments [9, 50]; sector dephasing drives a fast-scrambling example [51]; the trace-distance analysis separates sector coherences and a residual in collective models [52]; frozen fragments provide a distinct boundary mechanism [53]. Subsystem-charge fluctuations probe entanglement [54–58] and were measured in the 12-ion data [59]. Here the finite-block no-go and threshold are complemented by the exact short-time transport split and a conditional crossing estimate. The record condition relates restoration to environment decoherence [60, 61] and applies, under (C1)–(C3), to one-axis twisting [62–66], condensate phase diffusion [67, 68] and cavity-dephased qubits [69, 70]. Equation (8) predicts short-time density redistribution for any array with varying row sums; its crossing consequences require case-by-case checks. Open remain an applicability test for the collective conversion, the experimental excess edge dephasing, and a von Neumann no-go proof. A tilt-resolved 51-ion run recording block populations and single-site coherences would test Eq. (9).

We thank the authors of Refs. [15, 25] for making their raw data public. All analysis code and derived data are provided as Supplemental Material.

[1] E. B. Mpemba and D. G. Osborne, Cool?, Phys. Educ. **4**, 172 (1969).
[2] G. Teza, J. Bechhoefer, A. Lasanta, O. Raz, and M. Vucelja, Speedups in nonequilibrium thermal relaxation: Mpemba and related effects, Phys. Rep. **1164**, 1 (2026).
[3] Z. Lu and O. Raz, Nonequilibrium thermodynamics of the Markovian Mpemba effect and its inverse, Proc. Natl. Acad. Sci. U.S.A. **114**, 5083 (2017).
[4] A. Kumar and J. Bechhoefer, Exponentially faster cooling in a colloidal system, Nature **584**, 64 (2020).
[5] F. Carollo, A. Lasanta, and I. Lesanovsky, Exponentially accelerated approach to stationarity in Markovian open quantum systems through the Mpemba effect, Phys. Rev. Lett. **127**, 060401 (2021).
[6] F. Ares, S. Murciano, and P. Calabrese, Entanglement asymmetry as a probe of symmetry breaking, Nat. Commun. **14**, 2036 (2023).
[7] F. Ares, S. Murciano, E. Vernier, and P. Calabrese, Lack of symmetry restoration after a quantum quench: An entanglement asymmetry study, SciPost Phys. **15**, 089 (2023).
[8] S. Murciano, F. Ares, I. Klich, and P. Calabrese, Entanglement asymmetry and quantum Mpemba effect in the XY spin chain, J. Stat. Mech. **2024**, 013103 (2024).
[9] C. Rylands, K. Klobas, F. Ares, P. Calabrese, S. Murciano, and B. Bertini, Microscopic origin of the quantum Mpemba effect in integrable systems, Phys. Rev. Lett. **133**, 010401 (2024).
[10] K. Chalas, F. Ares, C. Rylands, and P. Calabrese, Multiple crossings during dynamical symmetry restoration and implications for the quantum Mpemba effect, J. Stat. Mech. **2024**, 103101 (2024).
[11] S. Yamashika, F. Ares, and P. Calabrese, Entanglement asymmetry and quantum Mpemba effect in two-dimensional free-fermion systems, Phys. Rev. B **110**, 085126 (2024).
[12] S. Liu, H.-K. Zhang, S. Yin, and S.-X. Zhang, Symmetry restoration and quantum Mpemba effect in symmetric random circuits, Phys. Rev. Lett. **133**, 140405 (2024).

[13] X. Turkeshi, P. Calabrese, and A. De Luca, Quantum Mpemba effect in random circuits, Phys. Rev. Lett. **135**, 040403 (2025).

[14] F. Ares, P. Calabrese, and S. Murciano, The quantum Mpemba effects, Nat. Rev. Phys. **7**, 451 (2025).

[15] L. Kh. Joshi, J. Franke, A. Rath, F. Ares, S. Murciano, F. Kranzl, R. Blatt, P. Zoller, B. Vermersch, P. Calabrese, C. F. Roos, and M. K. Joshi, Observing the quantum Mpemba effect in quantum simulations, Phys. Rev. Lett. **133**, 010402 (2024).

[16] A. Nava and R. Egger, Mpemba effects in open nonequilibrium quantum systems, Phys. Rev. Lett. **133**, 136302 (2024).

[17] M. Moroder, O. Culhane, K. Zawadzki, and J. Goold, Thermodynamics of the quantum Mpemba effect, Phys. Rev. Lett. **133**, 140404 (2024).

[18] S. Aharony Shapira, Y. Shapira, J. Markov, G. Teza, N. Akerman, O. Raz, and R. Ozeri, Inverse Mpemba effect demonstrated on a single trapped ion qubit, Phys. Rev. Lett. **133**, 010403 (2024).

[19] J. Zhang, G. Xia, C.-W. Wu, T. Chen, Q. Zhang, Y. Xie, W.-B. Su, W. Wu, C.-W. Qiu, P.-X. Chen, W. Li, H. Jing, and Y.-L. Zhou, Observation of quantum strong Mpemba effect, Nat. Commun. **16**, 301 (2025).

[20] Z. Wei, M. Xu, Y. Song, X.-P. Jiang, Y. Yan, and L. Pan, Symmetry-filtered relaxation comb and strong quantum Mpemba effect in long-range XXZ spin chains, arXiv:2605.20930 (2026).

[21] A. Hallam, M. Yusuf, A. A. Clerk, I. Martin, and Z. Papić, Tunable quantum Mpemba effect in long-range interacting systems, Phys. Rev. B **114**, 125135 (2026).

[22] H.-Z. Li, C. H. Lee, S. Liu, S.-X. Zhang, and J.-X. Zhong, Quantum Mpemba effect in long-ranged U(1)-symmetric random circuits, arXiv:2512.06775 (2025).

[23] C. Rylands, E. Vernier, and P. Calabrese, Dynamical symmetry restoration in the Heisenberg spin chain, J. Stat. Mech. **2024**, 123102 (2024).

[24] S. Yamashika and F. Ares, Quantum Mpemba effect in long-range spin systems, Phys. Rev. Lett. **136**, 090402 (2026).

[25] J. Franke, S. R. Muleady, R. Kaubruegger, F. Kranzl, R. Blatt, A. M. Rey, M. K. Joshi, and C. F. Roos, Quantum-enhanced sensing on optical transitions through finite-range interactions, Nature **621**, 740 (2023).

[26] See Supplemental Material for the proofs of Theorem 1, Corollary 1 and Propositions 1–3, Theorem S1, the transport analysis, the data analysis and validation for both experiments, the tensor-network and discrete truncated Wigner simulations and their convergence, and the measurement protocols, which includes Refs. [93, 94].

[27] C. O'Meara and R. Pereira, Self-dual maps and symmetric bistochastic matrices, Linear Multilinear Algebra **61**, 23 (2013).

[28] L. J. Landau and R. F. Streater, On Birkhoff's theorem for doubly stochastic completely positive maps of matrix algebras, Linear Algebra Appl. **193**, 107 (1993).

[29] J. Helm and W. T. Strunz, Quantum decoherence of two qubits, Phys. Rev. A **80**, 042108 (2009).

[30] U. Grenander and G. Szegő, *Toeplitz Forms and Their Applications* (University of California Press, Berkeley, 1958).

[31] M.-D. Choi, Completely positive linear maps on complex matrices, Linear Algebra Appl. **10**, 285 (1975).

[32] M. A. Nielsen and I. L. Chuang, *Quantum Computation and Quantum Information*, 10th ed. (Cambridge University Press, Cambridge, England, 2010).

[33] M. Kitagawa and M. Ueda, Squeezed spin states, Phys. Rev. A **47**, 5138 (1993).

[34] M. Foss-Feig, K. R. A. Hazzard, J. J. Bollinger, and A. M. Rey, Nonequilibrium dynamics of arbitrary-range Ising models with decoherence: An exact analytic solution, Phys. Rev. A **87**, 042101 (2013).

[35] I.-S. Yang, The entanglement timescale, Phys. Rev. D **97**, 066008 (2018), arXiv:1707.05792 [hep-th].

[36] D. Porras and J. I. Cirac, Effective quantum spin systems with trapped ions, Phys. Rev. Lett. **92**, 207901 (2004).

[37] C. Monroe, W. C. Campbell, L.-M. Duan, Z.-X. Gong, A. V. Gorshkov, P. W. Hess, R. Islam, K. Kim, N. M. Linke, G. Pagano, P. Richerme, C. Senko, and N. Y. Yao, Programmable quantum simulations of spin systems with trapped ions, Rev. Mod. Phys. **93**, 025001 (2021).

[38] P. Jurcevic, B. P. Lanyon, P. Hauke, C. Hempel, P. Zoller, R. Blatt, and C. F. Roos, Quasiparticle engineering and entanglement propagation in a quantum many-body system, Nature **511**, 202 (2014).

[39] P. Richerme, Z.-X. Gong, A. Lee, C. Senko, J. Smith, M. Foss-Feig, S. Michalakis, A. V. Gorshkov, and C. Monroe, Non-local propagation of correlations in quantum systems with long-range interactions, Nature **511**, 198 (2014).

[40] M. K. Joshi, F. Kranzl, A. Schuckert, I. Lovas, C. Maier, R. Blatt, M. Knap, and C. F. Roos, Observing emergent hydrodynamics in a long-range quantum magnet, Science **376**, 720 (2022).

[41] A. Elben, S. T. Flammia, H.-Y. Huang, R. Kueng, J. Preskill, B. Vermersch, and P. Zoller, The randomized measurement toolbox, Nat. Rev. Phys. **5**, 9 (2023).

[42] T. Brydges, A. Elben, P. Jurcevic, B. Vermersch, C. Maier, B. P. Lanyon, P. Zoller, R. Blatt, and C. F. Roos, Probing Rényi entanglement entropy via randomized measurements, Science **364**, 260 (2019).

[43] H.-Y. Huang, R. Kueng, and J. Preskill, Predicting many properties of a quantum system from very few measurements, Nat. Phys. **16**, 1050 (2020).

[44] F. Kranzl, M. K. Joshi, C. Maier, T. Brydges, J. Franke, R. Blatt, and C. F. Roos, Controlling long ion strings for quantum simulation and precision measurements, Phys. Rev. A **105**, 052426 (2022).

[45] J. Haegeman, C. Lubich, I. Oseledets, B. Vandereycken, and F. Verstraete, Unifying time evolution and optimization with matrix product states, Phys. Rev. B **94**, 165116 (2016).

[46] J. Hauschild and F. Pollmann, Efficient numerical simulations with tensor networks: Tensor network Python (TeNPy), SciPost Phys. Lect. Notes , 5 (2018).

[47] J. Schachenmayer, A. Pikovski, and A. M. Rey, Many-body quantum spin dynamics with Monte Carlo trajectories on a discrete phase space, Phys. Rev. X **5**, 011022 (2015).

[48] A. Polkovnikov, Phase space representation of quantum dynamics, Ann. Phys. (N.Y.) **325**, 1790 (2010).

[49] S. R. Muleady, M. Yang, S. R. White, and A. M. Rey, Validating phase-space methods with tensor networks in two-dimensional spin models with power-law interactions, Phys. Rev. Lett. **131**, 150401 (2023).

[50] B. Bertini, K. Klobas, M. Collura, P. Calabrese, and C. Rylands, Dynamics of charge fluctuations from asymmetric initial states, Phys. Rev. B **109**, 184312 (2024).

[51] S. Cao and X.-H. Ge, Symmetry restoration in a fast scrambling system, arXiv:2509.26176 (2025).

[52] T. S, M. C, B. K. Agarwalla, and U. Divakaran, Symmetry structure dependent diagnostic of the quantum Mpemba effect, arXiv:2609.10470 (2026).

[53] S. Aditya, S. Murciano, and X. Turkeshi, Higher-order symmetric quantum Mpemba effect in fragmented systems, arXiv:2606.06653 (2026).

[54] I. Klich and L. Levitov, Quantum noise as an entanglement meter, Phys. Rev. Lett. **102**, 100502 (2009).

[55] H. F. Song, S. Rachel, C. Flindt, I. Klich, N. Laflorencie, and K. Le Hur, Bipartite fluctuations as a probe of many-body entanglement, Phys. Rev. B **85**, 035409 (2012).

[56] M. Goldstein and E. Sela, Symmetry-resolved entanglement in many-body systems, Phys. Rev. Lett. **120**, 200602 (2018).

[57] J. C. Xavier, F. C. Alcaraz, and G. Sierra, Equipartition of the entanglement entropy, Phys. Rev. B **98**, 041106(R) (2018).

[58] L. S. Levitov, H. Lee, and G. B. Lesovik, Electron counting statistics and coherent states of electric current, J. Math. Phys. **37**, 4845 (1996).

[59] L. Kh. Joshi, F. Ares, M. K. Joshi, C. F. Roos, and P. Calabrese, Measuring full counting statistics in a trapped-ion quantum simulator, Phys. Rev. Lett. **135**, 160601 (2025).

[60] W. H. Zurek, Decoherence, einselection, and the quantum origins of the classical, Rev. Mod. Phys. **75**, 715 (2003).

[61] G. M. Palma, K.-A. Suominen, and A. K. Ekert, Quantum computers and dissipation, Proc. R. Soc. Lond. A **452**, 567 (1996).

[62] J. G. Bohnet, B. C. Sawyer, J. W. Britton, M. L. Wall, A. M. Rey, M. Foss-Feig, and J. J. Bollinger, Quantum spin dynamics and entanglement generation with hundreds of trapped ions, Science **352**, 1297 (2016).

[63] G. Bornet, G. Emperauger, C. Chen, B. Ye, M. Block, M. Bintz, J. A. Boyd, D. Barredo, T. Comparin, F. Mezzacapo, T. Roscilde, T. Lahaye, N. Y. Yao, and A. Browaeys, Scalable spin squeezing in a dipolar Rydberg atom array, Nature **621**, 728 (2023).

[64] W. J. Eckner, N. Darkwah Oppong, A. Cao, A. W. Young, W. R. Milner, J. M. Robinson, J. Ye, and A. M. Kaufman, Realizing spin squeezing with Rydberg interactions in an optical clock, Nature **621**, 734 (2023).

[65] J. A. Hines, S. V. Rajagopal, G. L. Moreau, M. D. Wahrman, N. A. Lewis, O. Marković, and M. Schleier-Smith, Spin squeezing by Rydberg dressing in an array of atomic ensembles, Phys. Rev. Lett. **131**, 063401 (2023).

[66] M. Block, B. Ye, B. Roberts, S. Chern, W. Wu, Z. Wang, L. Pollet, E. J. Davis, B. I. Halperin, and N. Y. Yao, Scalable spin squeezing from finite-temperature easy-plane magnetism, Nat. Phys. **20**, 1575 (2024).

[67] M. Lewenstein and L. You, Quantum phase diffusion of a Bose-Einstein condensate, Phys. Rev. Lett. **77**, 3489 (1996).

[68] Y. Castin and J. Dalibard, Relative phase of two Bose-Einstein condensates, Phys. Rev. A **55**, 4330 (1997).

[69] J. Gambetta, A. Blais, D. I. Schuster, A. Wallraff, L. Frunzio, J. Majer, M. H. Devoret, S. M. Girvin, and R. J. Schoelkopf, Qubit-photon interactions in a cavity: Measurement-induced dephasing and number splitting, Phys. Rev. A **74**, 042318 (2006).

[70] D. I. Schuster, A. A. Houck, J. A. Schreier, A. Wallraff, J. M. Gambetta, A. Blais, L. Frunzio, J. Majer, B. Johnson, M. H. Devoret, S. M. Girvin, and R. J. Schoelkopf, Resolving photon number states in a superconducting circuit, Nature **445**, 515 (2007).

[71] J. Baum, M. Munowitz, A. N. Garroway, and A. Pines, Multiple-quantum dynamics in solid state NMR, J. Chem. Phys. **83**, 2015 (1985).

[72] T. Comparin, F. Mezzacapo, and T. Roscilde, Robust spin squeezing from the tower of states of U(1)-symmetric spin Hamiltonians, Phys. Rev. A **105**, 022625 (2022).

[73] T. Comparin, F. Mezzacapo, and T. Roscilde, Multipartite entangled states in dipolar quantum simulators, Phys. Rev. Lett. **129**, 150503 (2022).

[74] D. Crow and R. Joynt, Classical simulation of quantum dephasing and depolarizing noise, Phys. Rev. A **89**, 042123 (2014).

[75] N. Defenu, T. Donner, T. Macrì, G. Pagano, S. Ruffo, and A. Trombettoni, Long-range interacting quantum systems, Rev. Mod. Phys. **95**, 035002 (2023).

[76] M. Foss-Feig, Z.-X. Gong, C. W. Clark, and A. V. Gorshkov, Nearly linear light cones in long-range interacting quantum systems, Phys. Rev. Lett. **114**, 157201 (2015).

[77] M. Gärttner, J. G. Bohnet, A. Safavi-Naini, M. L. Wall, J. J. Bollinger, and A. M. Rey, Measuring out-of-time-order correlations and multiple quantum spectra in a trapped-ion quantum magnet, Nat. Phys. **13**, 781 (2017).

[78] S. J. Harris, R. H. Levene, V. I. Paulsen, S. Plosker, and M. Rahaman, Schur multipliers and mixed unitary maps, J. Math. Phys. **59**, 112201 (2018).

[79] P. Hauke and L. Tagliacozzo, Spread of correlations in long-range interacting quantum systems, Phys. Rev. Lett. **111**, 207202 (2013).

[80] J. Kattemölle and J. van Wezel, Conditions for superdecoherence, Quantum **4**, 265 (2020).

[81] A. Lerose and S. Pappalardi, Origin of the slow growth of entanglement entropy in long-range interacting spin systems, Phys. Rev. Res. **2**, 012041 (2020).

[82] J. Ma, X. Wang, C. P. Sun, and F. Nori, Quantum spin squeezing, Phys. Rep. **509**, 89 (2011).

[83] T. Monz, P. Schindler, J. T. Barreiro, M. Chwalla, D. Nigg, W. A. Coish, M. Harlander, W. Hänsel, M. Hennrich, and R. Blatt, 14-qubit entanglement: Creation and coherence, Phys. Rev. Lett. **106**, 130506 (2011).

[84] G. A. Paz-Silva, L. M. Norris, and L. Viola, Multiqubit spectroscopy of Gaussian quantum noise, Phys. Rev. A **95**, 022121 (2017).

[85] M. A. Perlin, C. Qu, and A. M. Rey, Spin squeezing with short-range spin-exchange interactions, Phys. Rev. Lett. **125**, 223401 (2020).

[86] L. Pezzè, A. Smerzi, M. K. Oberthaler, R. Schmied, and P. Treutlein, Quantum metrology with nonclassical states of atomic ensembles, Rev. Mod. Phys. **90**, 035005 (2018).

[87] A. Rath, V. Vitale, S. Murciano, M. Votto, J. Dubail, R. Kueng, C. Branciard, P. Calabrese, and B. Vermersch, Entanglement barrier and its symmetry resolution: Theory and experimental observation, PRX Quantum **4**, 010318 (2023).

[88] T. Roscilde, T. Comparin, and F. Mezzacapo, Entangling dynamics from effective rotor–spin-wave separation in U(1)-symmetric quantum spin models, Phys. Rev. Lett. **131**, 160403 (2023).

[89] T. Roscilde, T. Comparin, and F. Mezzacapo, Rotor/spin-wave theory for quantum spin models with U(1) symmetry, Phys. Rev. B **108**, 155130 (2023).

[90] R. Senese, J. H. Robertson, and F. H. L. Essler, Out-of-equilibrium full counting statistics in Gaussian theories

of quantum magnets, SciPost Phys. **17**, 139 (2024).
[91] P. Szańkowski, G. Ramon, J. Krzywda, D. Kwiatkowski, and Ł. Cywiński, Environmental noise spectroscopy with qubits subjected to dynamical decoupling, J. Phys.: Condens. Matter **29**, 333001 (2017).
[92] U. von Lüpke, F. Beaudoin, L. M. Norris, Y. Sung, R. Winik, J. Y. Qiu, M. Kjaergaard, D. Kim, J. Yoder, S. Gustavsson, L. Viola, and W. D. Oliver, Two-qubit spectroscopy of spatiotemporally correlated quantum noise in superconducting qubits, PRX Quantum **1**, 010305 (2020).
[93] G. Lindblad, On the generators of quantum dynamical semigroups, Commun. Math. Phys. **48**, 119 (1976).
[94] D. J. Wineland, J. J. Bollinger, W. M. Itano, and D. J. Heinzen, Squeezed atomic states and projection noise in spectroscopy, Phys. Rev. A **50**, 67 (1994).